Electric Power Systems Research 180 (2020) 106107

Contents lists available at ScienceDirect

Electric Power Systems Research

journal homepage: www.elsevier.com/locate/epsr

Identifying the root cause of power system disturbances based on waveform templates

Yuanqian Ma[a], Xianyong Xiao[b], Yang Wang[b,*]

[a] Faculty of Mechanical Engineering & Automation, Zhejiang Sci-Tech University, 310018 Hangzhou, China
[b] The College of Electrical Engineering, Sichuan University, 610065 Chengdu, China

ARTICLE INFO

Keywords:
Power system disturbances
Root cause identification
Energization events
Waveform templates

ABSTRACT

Most existing work related with power disturbance identification focuses on the classification of power disturbances, i.e. to identify the type of the power disturbances. It is however more important to know the root cause of the power disturbance when troubleshooting or responsibility assignment is required. For this purpose, a novel time-domain method is proposed in this paper for the root cause identification. The basic idea is to develop the waveform templates for describing each power disturbances of concern and then use the templates to fit the disturbances measured at the substation. Three common power system energization events including capacitor energization, no-load transformer energization, and motor starting, are investigated. All these events induce large currents to the system, thus are very likely to cause power quality issues. The effectiveness of the proposed method has been verified thoroughly using PSCAD/EMTDC simulations, lab experiment and field data.

1. Introduction

The power quality problem is, in its essence, caused by power quality disturbances. Poor power quality adversely affects both power system components and customers' devices. Thus, it is necessary to timely detect and identify the disturbances. In the past few years, lots of methods have been developed for feature extraction [1–6] and classification [7–12] of power disturbances. These methods can tell the engineers about the type of power disturbances, but it is not sufficient for troubleshooting [3]. When a power disturbance causes the problem, it is more important to know root causes of the disturbances. Only after the root cause is identified correctly, appropriate mitigating actions can be taken and responsibility can be assigned.

For this purpose, some efforts have been made recently on the identification of the root cause of power disturbances. Reference [13] uses rule-based expert system to identify three power quality events, i.e. converter operation, transformer energization and capacitor energization based on the features extracted by Fourier and wavelet transforms. In Ref. [14], a method based on wavelet transform is proposed to discriminate a fault and a capacitor-switching incident. Similarly [15], uses wavelet transform with rank correlation and the fuzzy technique to identify capacitor switching transients. It can be found that all above methods use Fourier or/and wavelet transform to identify the root cause of power disturbances. The Fourier transform is developed for stationary signals, thus its performance cannot be guaranteed when applied for transient disturbances. On the other hand, wavelet transform can only provide the frequency range, rather than the main oscillation frequency due to spectral leakage [16]. The performance of the wavelet transform also highly depends on the number of decomposition layers and the choice of wavelet bases [17]. A more advanced method based on *s*-transform and extreme learning machine is proposed in Ref. [18]. The method is developed to recognize the underlying causes of power quality events, including fault event, self-extinguishing fault event, non-fault interruption event and transformer energizing event. However, machine learning based methods are generally complex, which is not straightforward for field engineers to use. Besides, the classification accuracy of the method highly depends on the training sample size. For different systems, different training processes are needed.

This paper proposes a time-domain method to identify the root cause of power disturbances. The basic idea is to first develop waveform templates for different power disturbances based on their signatures and then identify the root cause through the pattern match. Three most common energizing events including capacitor energization, no-load transformer energization and motor starting are studied in this paper. These events all induce large currents, leading to serious power quality concerns. With respect to previous work, the main contributions of this work are (1) the proposed method is time-domain based, thus can be

* Corresponding author.
E-mail address: fwang@scu.edu.cn (Y. Wang).

https://doi.org/10.1016/j.epsr.2019.106107
Received 26 July 2019; Accepted 4 November 2019
Available online 26 November 2019
0378-7796/

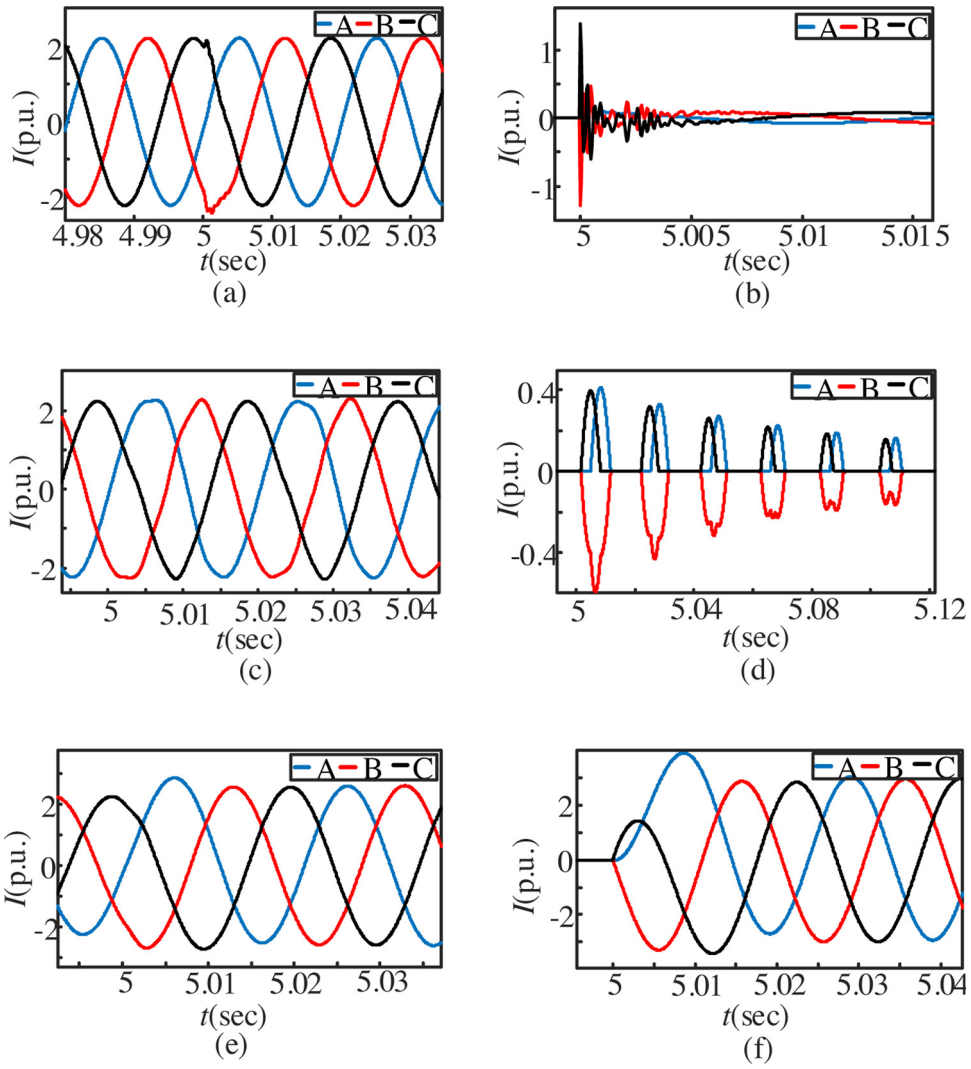

Fig. 1. Three-phase current waveforms with power disturbances. (a) Capacitor energization current observed at the substation. (b) Capacitor energization current observed at the original location. (c) No-load transformer energization current observed at the substation. (d) No-load transformer energization current observed at the original location. (e) Motor starting current observed at the substation. (f) Motor starting current observed at the original location.

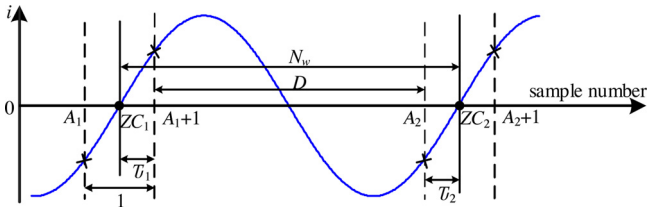

Fig. 2. Parameters for frequency variation correction.

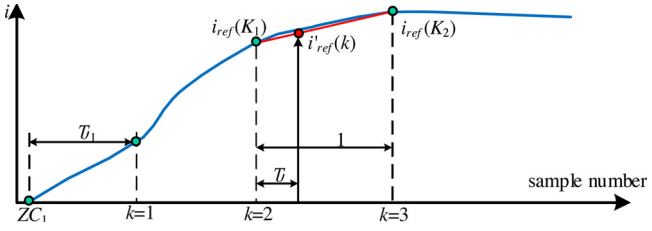

Fig. 3. Determining the value of $i'_{ref}(k)$.

applied to both stationary and transient signals; (2) the proposed method can provide detailed information about the disturbance, which is useful for post-analysis; (3) the proposed method is simple and straightforward for field engineers to use.

The remainder of the paper is organized as follows. Section 2 explains the idea of the proposed method. Section 3 presents the developed templates for three disturbances. Simulation study, laboratory test verification, and field data verification results are shown in Sections 4–6. Finally, conclusions are drawn in Section 7.

2. Proposed method

The proposed method consists of two steps. First, abnormal waveforms are detected and extracted from the measurements. The abnormal waveforms are defined as waveforms including power disturbances. Then, the extracted abnormal waveform is compared with the "templates" that previously developed for different energizing events. The root cause can be identified if the measured waveform matches the template well. Since the energization transients are more visible in current waveforms than voltage waveforms [19,20], the following paper uses current waveforms for the root cause identification.

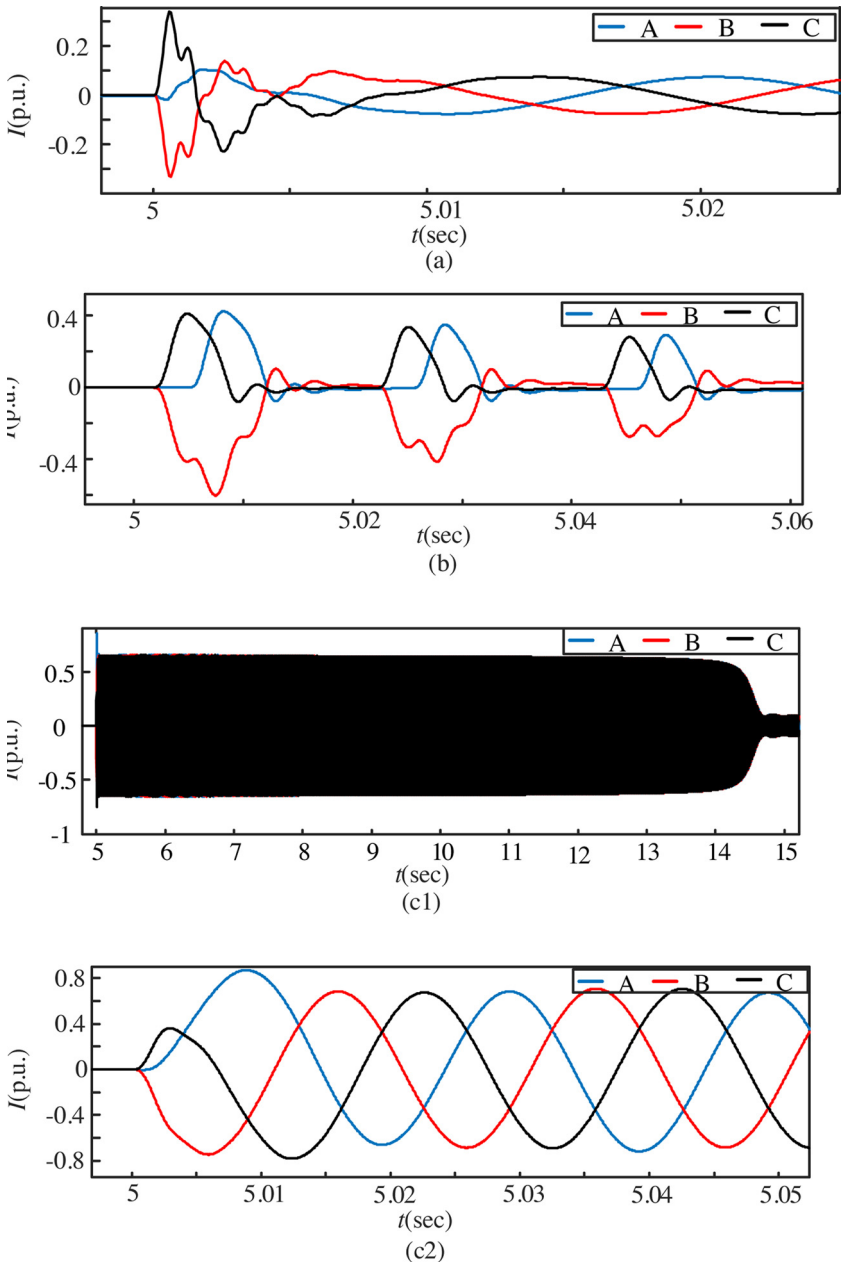

Fig. 4. Three-phase residual current waveforms. (a) Capacitor energization. (b) No-load transformer energization. (c1) Motor starting. (c2) The enlarged waveform of (c1).

2.1. Detection and extraction of abnormal waveforms

This paper adopts the method in Ref. [19] to detect the abnormal waveform. The method is briefly explained as follows. First, the statistical distributions of waveform variations with and without power disturbances are calculated. Then, Kullback–Leibler divergence (KLD) is used to assess the difference of the distributions. An abnormal waveform (i.e. the waveform with power disturbance) is detected if the KLD is larger than a threshold. The abnormal waveform data will then be saved for further analysis in the format of three cycles' pre-disturbance data, the entire disturbance data and three cycles' post-disturbance data. The length of data window depends on the duration of the disturbance. For capacitor energization, the duration is about 5 μs–50 ms. For no-load transformer energization, the duration is about half cycle to 1 min. For motor starting, the duration ranges from several seconds to several minutes. In short, the length of time window is determined as "3 cycles' pre-disturbance + disturbance + 3 cycles' post-disturbance".

Fig. 1 shows the abnormal waveforms caused by three energizing events. These waveforms are generated by simulations and detected by the method in Ref. [19] at the original location (the location of the energizing event) as well as the remote substation. It can be seen that the waveforms of different energizing events exhibit distinguishable characteristics at their original locations. However, these characteristics become ambiguous at the remote substation.

Once the abnormal waveform is detected, the next step is to extract the disturbance. This can be realized by the subtraction between the saved waveform and the first cycle of the saved waveform, i.e. all the cycles of the saved waveform subtract the first cycle of the saved waveform. After subtraction, the obtained waveform is called the residual current waveform. Note the operating frequency of a power system seldom stays exactly at 60 Hz or 50 Hz [21]. Two waveforms to be subtracted thus have to be synchronized with the exact system frequency. This can be realized by means of hardware sampling synchronization [22,23] or software resampling methods [24]. The latter

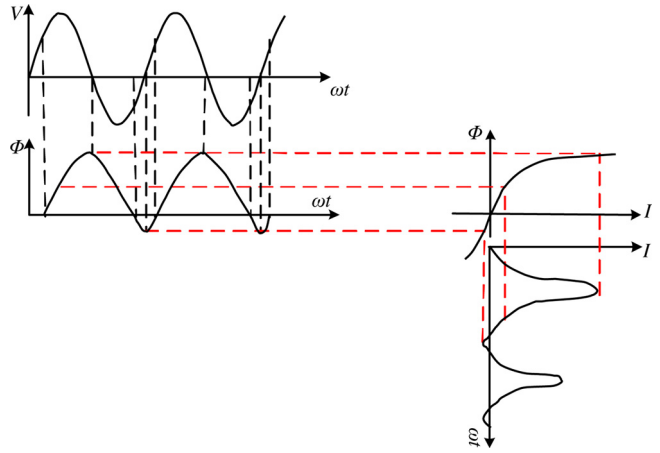

Fig. 5. The relationship between the inrush current and the magnetic flux.

one is adopted in this paper to address the frequency variation issue. The detailed steps are explained as follows.

1) The first cycle of the saved current waveform is selected as the reference cycle.
2) Determine the positive zero-crossing point ZC_1 of the first cycle, shown in Fig. 2. The location of ZC_1 lies between a sample with a negative value (A_1) and the next sample with a positive value ($A_1 + 1$). The fraction difference between samples $A_1 + 1$ and ZC_1, which is labeled as τ_1. τ_1 is less than 1.
3) Determine the positive zero-crossing point ZC_2 of the second cycle. The value of ZC_2 lies between sample points A_2 and $A_2 + 1$. The fraction difference between samples A_2 and ZC_2 is called τ_2. Note that τ_1 is a fraction between ZC_1 and $A_1 + 1$ while τ_2 is between A_2 and ZC_2 (not ZC_2 and $A_2 + 1$). τ_2 is also less than 1.
4) The precise period of the waveform, T_w, can then be calculated from:

$$T_w = [A_2 - (A_1 + 1) + \tau_1 + \tau_2] \times \Delta t = [D + \tau_1 + \tau_2] \times \Delta t = N_w \times \Delta t \tag{1}$$

where, Δt is the sampling time interval.

5) For any point $i(k)$ on the waveform, we want to resample a corresponding point $i_{ref}(k)$ in the reference cycle whose phase angle is the same as $i(k)$. To achieve this, the first step is to compute the time difference between $i(k)$ and the positive zero crossing point of the reference cycle, ZC_1, as follows:

$$T_{diff} = (k - ZC_1)\Delta t \tag{2}$$

The number of cycles separating the two instants is:

$$N_{diff} = (k - ZC_1)\Delta t / T_w = (k - ZC_1)/N_w \tag{3}$$

Note that N_{diff} is not an integer. Its remainder, denoted as N_R, represents the sample location where $i'_{ref}(k)$ should be calculated. N_R resides between 0.0 to 1.0. If $N_R = 0.5$, it means that $i'_{ref}(k)$ is located at the exact mid-point of the reference cycle.

6) The N_R value can then be used to find the two adjacent samples in the reference cycle that should be used to calculate $i'_{ref}(k)$. To do this, we first compute N'_r as follows:

$$N'_r = N_R \times N_w - \tau_1 + 1 \tag{4}$$

The value of N'_r will reside between two integers. These two integers are recorded as K_1 and K_2. The remainder of N'_r is recorded as τ. For example, if $N'_r = 5.34$, one will have $K_1 = 5$, $K_2 = 6$ and $\tau = 0.34$. The value of $i'_{ref}(k)$ is computed from linear interpolation of $i_{ref}(K_1)$ and $i_{ref}(K_2)$ as shown in Fig. 3. The equation is as follows.

$$i'_{ref}(k) = i_{ref}(K_1) + \tau[i_{ref}(K_2) - i_{ref}(K_1)] \tag{5}$$

If $K_1 = 0$, the first point is the ZC_1 so the value of $i_{ref}(K_1) = 0$. If K_1 is the last sample of the reference cycle, the interpolation should take place between K_1 and ZC_2.

7) Finally, the residual current can be obtained by Eq. (6). Repeat Step 3) to 7) for every sample points to obtain the residual current waveform.

$$\Delta i(k) = i(k) - i'_{ref}(k) \tag{6}$$

The performance of the above method is found to be satisfactory, as shown in Fig. 4.

2.2. Strategy for root cause identification

As seen from Fig. 4, the residual current for capacitor energization, no-load transformer energization, and motor starting exhibit similar waveform shapes as the current measured at the original location (see Fig. 1). This is because the travelling path of disturbances from original location to the substation is actually a linear circuit. The linear circuit only changes the magnitude of the disturbance at different frequencies, but the constitution of the waveforms remains the same. In other words, no matter of the grid parameters, the mathematical model for the same kind of energization event is the same. The difference resulting from system parameters lies on the magnitude, oscillation frequency and damping factor of the waveform, i.e. the parameters of the mathematical model. Based on the above finding, this paper attempts to develop templates for describing each power disturbance of concern, and then matches the disturbances detected at the substation with the templates. This is the subject of the next section.

3. Templates for three energizing events

In this section, the templates for capacitor energization, no-load transformer energization, and motor starting are developed first. Then the procedure to implement the proposed method is explained.

3.1. Template for capacitor energization

The capacitor is switched on and off routinely in power systems to support voltage or correct power factor. The interaction between the capacitor and the system inductance results in high frequency oscillations [25]. A sudden increase in voltage to the inductive load results in DC components [15]. As seen from Fig. 4(a), the residual current waveform of capacitor energization consists of three parts, i.e. steady-state sinusoidal component, decaying DC component, and decaying high frequency oscillation component. Therefore, the template of the residual current waveform for capacitor energization can be represented by Eq. (7).

$$I_{resid-capacitor} = A_{1c}e^{-\alpha_{1c}t} + A_{2c}e^{-\alpha_{2c}t}\cos(\omega_{2c}t + \theta_{2c}) + A_{3c}\cos(\omega_{3c}t + \theta_{3c}) \tag{7}$$

In Eq. (7), the first term represents the decaying DC component, the second term represents the decaying high frequency oscillation component and the last term represents the steady-state sinusoidal component. A_{1c}, A_{2c} and A_{3c} are the magnitude, α_{1c} and α_{2c} are the damping factor, ω_{2c} and ω_{3c} are the oscillation frequency, and θ_{2c} and θ_{3c} are the initial phase angle. All these parameters are unknown and least-squares estimation [26] are then used to fit the measured disturbance with the template.

3.2. Template for no-load transformer energization

When a no-load transformer is energized, the high inrush current occurs due to saturation effects in the transformer iron core. Inrush

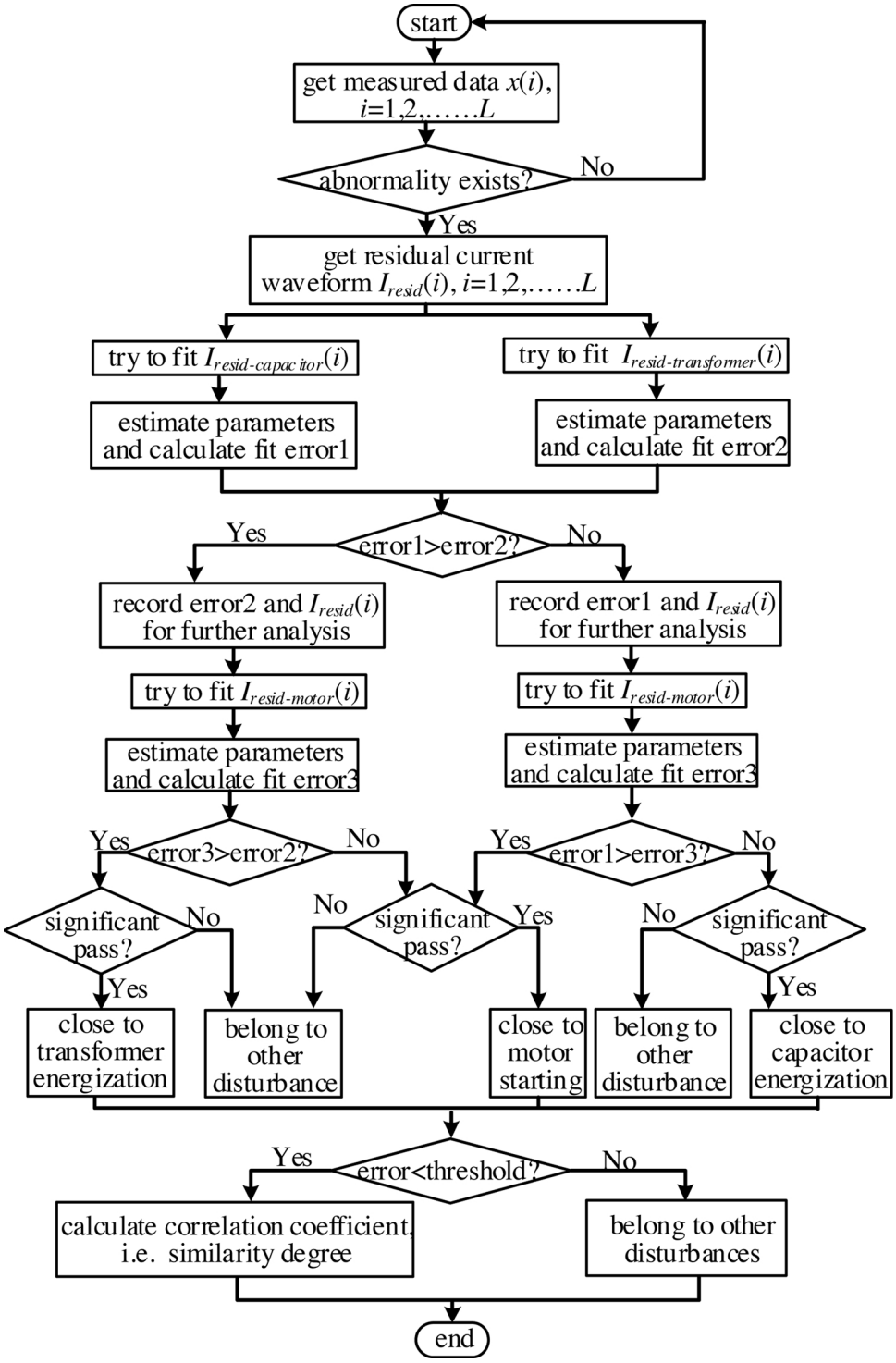

Fig. 6. The flowchart of identifying capacitor energization, no-load transformer energization, and motor starting.

currents contain significant odd and even harmonics, mainly from 2nd to 5th harmonics [13]. There is also a large part of DC component due to attempted instantaneous changes in the current through an inductor [27].

As seen from Fig. 4(b), the residual current waveform for no-load transformer energization can be divided into several segments. Each segment looks like an individual decaying oscillation. The oscillations in different segments have similar shapes but with reduced initial energy. This phenomenon can be explained as follows. The system voltage varies at the power frequency and the integral of the voltage yields the magnetic flux. Considering the relationship between the inrush current and the magnetic flux shown in Fig. 5, each segment should correspond to one power frequency cycle. The initial energy of each segment decays due to the damping effect of the system. Thus, the number of data points in each segment is $M = 1/(\Delta t \times f_0)$ and the segment number can be obtained as $K = L/M$, where L is the number of total data points, f_0 is the power frequency, and Δt is the sampling time interval. The sample time t and the corresponding current value $I_{resid\text{-}transformer}$ can be represented in the form of matrix, i.e. $t = [t_{ik}]_{M\times K}$, $I_{resid\text{-}transformer} = [m_{ik}]_{M\times K}$.

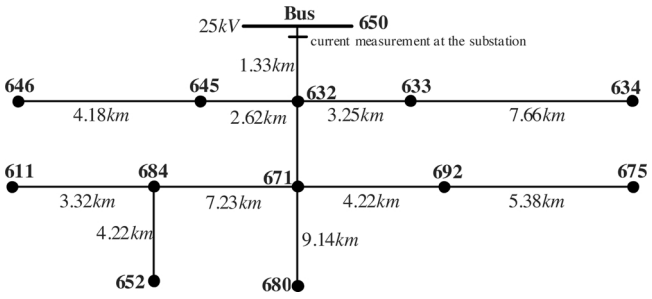

Fig. 7. The modified IEEE-13 node test feeder.

For each segment, the residual current waveform can be represented by Eq. (8).

$$I_{resid-transformer}(i,\,k) = g(i,\,k) * \tilde{\delta}_T(i,\,k) + A_{1t}(k)\cos\left[\omega(k)t_{ik} + \theta_{1t}(k)\right] \tag{8}$$

where,

$$\begin{aligned} g(i,\,k) = {} & A_{2t}(k)e^{-\alpha_{2t}(k)\times t_{ik}}\cos\left[2\omega(k)t_{ik} + \theta_{2t}(k)\right] \\ & + A_{3t}(k)e^{-\alpha_{3t}(k)\times t_{ik}}\cos\left[3\omega(k)t_{ik} + \theta_{3t}(k)\right] \\ & + A_{4t}(k)e^{-\alpha_{4t}(k)\times t_{ik}}\cos\left[4\omega(k)t_{ik} + \theta_{4t}(k)\right] \\ & + A_{5t}(k)e^{-\alpha_{5t}(k)\times t_{ik}}\cos\left[5\omega(k)t_{ik} + \theta_{5t}(k)\right] + A_{0t}(k)e^{-\alpha_{0t}(k)\times t_{ik}} \end{aligned} \tag{9}$$

$$\tilde{\delta}_T(i,\,k) = e^{-\beta kT}\delta(t_{ik} - kT) \tag{10}$$

In (8), the first term represents the decaying DC component and 2nd to 5th harmonics, and the second term represents the steady-state sinusoidal component. $A_{1t}(k)$, $\omega(k)$ and $\theta_{1t}(k)$ represent the magnitude, angular frequency and the initial phase angle of the steady-state component in the k-th segment. $A_{2t}(k)$, $A_{3t}(k)$, $A_{4t}(k)$, $A_{5t}(k)$ and $A_{0t}(k)$ are the magnitude of the second, third, fourth, fifth order and DC component. $\alpha_{2t}(k)$, $\alpha_{3t}(k)$, $\alpha_{4t}(k)$, $\alpha_{5t}(k)$ and $\alpha_{0t}(k)$ are the corresponding damping factor. $\theta_{2t}(k)$, $\theta_{3t}(k)$, $\theta_{4t}(k)$, and $\theta_{5t}(k)$ are the corresponding initial phase angle. $\delta(t_{ik}\text{-}kT)$ is an impulse function with

$$\delta(t_{ik} - kT) = \begin{cases} 1 & t_{ik} = kT \\ 0 & t_{ik} \neq kT \end{cases} \tag{11}$$

The sign '*' denotes the convolution operation. The convolution result between $g(i,k)$ and $\tilde{\delta}_T(i,\,k)$ is shown in Eq. (12). It is clear that Eq. (12) represents the decaying DC component and 2nd to 5th harmonics with reduced initial energy for different segments.

$$\begin{aligned} & g(i,\,k) * \tilde{\delta}_T(i,\,k) \\ & = A_{2t}(k)e^{-[\alpha_{2t}(k)+\beta_{2t}(k)]t_{ik}}e^{\alpha_{2t}(k)kT}\cos\left[2\omega(k)(t_{ik} - kT) + \theta_{2t}(k)\right] \\ & + A_{3t}(k)e^{-[\alpha_{3t}(k)+\beta_{3t}(k)]t_{ik}}e^{\alpha_{3t}(k)kT}\cos\left[3\omega(k)(t_{ik} - kT) + \theta_{3t}(k)\right] \\ & + A_{4t}(k)e^{-[\alpha_{4t}(k)+\beta_{4t}(k)]t_{ik}}e^{\alpha_{4t}(k)kT}\cos\left[4\omega(k)(t_{ik} - kT) + \theta_{4t}(k)\right] \\ & + A_{5t}(k)e^{-[\alpha_{5t}(k)+\beta_{5t}(k)]t_{ik}}e^{\alpha_{5t}(k)kT}\cos\left[5\omega(k)(t_{ik} - kT) + \theta_{5t}(k)\right] \\ & + A_{0t}(k)e^{-[\alpha_{0t}(k)+\beta_{0t}(k)]t_{ik}}e^{\alpha_{0t}(k)kT} \end{aligned} \tag{12}$$

Similarly, all above parameters are unknown and least-squares estimation are used to fit the measured disturbance with the template.

3.3. Template for motor starting

Induction motors are one of the most common loads in power distribution systems. During the first stage of the motor starting, the motor draws a current that is about six or seven times of its full-load current due to the large slip. Then, the slip decreases slowly and the large current lasts until the motor is accelerated to 85% of the rated speed [28]. This can be regarded as the first phase of the motor starting, i.e. approximately from 5 s to 14 s in Fig. 4(c1). The disturbance waveform in this phase contains a large DC component due to suddenly applying voltage to the induction motor [29]. There is also a sinusoidal component at the power frequency with a decreasing magnitude. This decreasing can be modelled as a power function of the time [30].

After the motor reaches 85% of the rated speed, the current would decrease quickly until the motor reaches its rated speed [28]. This can be regarded as the second phase of the motor starting, i.e. the fast decaying oscillation component at the fundamental frequency, approximately from 14 s to 15 s in Fig. 4(c1).

Based on the above analysis, the template of the residual current waveform for the motor starting is developed as Eq. (13), where $f_1(t)$

Table 1
The estimation errors and the similarity degree of three phases.

Disturbance cause	Energize situation		Node 680	Node 611	Node 634
Capacitor	Size		0.19 MVar	0.639 MVar	0.23 MVar
	Instant		61.2°	0°	90°
	ε	A	3.5518×10^{-4}	5.9558×10^{-5}	0.0029
		B	6.2974×10^{-4}	0.0052	0.0013
		C	3.6997×10^{-6}	0.0058	7.0063×10^{-4}
	R	A	0.9998	1.0000	0.9985
		B	0.9997	0.9974	0.9993
		C	1.0000	0.9971	0.9996
	η		1	1	1
Transformer	Size		0.45 MVA	1.5 MVA	0.518 MVA
	Instant		77.85°	111.15°	0°
	ε	A	0.0040	0.0164	0.0031
		B	0.0031	0.0062	0.0053
		C	0.0057	0.0092	0.0075
	R	A	0.9980	0.9917	0.9984
		B	0.9984	0.9968	0.9973
		C	0.9971	0.9953	0.9962
	η		1	1	1
Motor	Size		452 kW	1.5 MVA	519 kW
	Instant		273.6°	16.65°	90°
	ε	A	7.2869×10^{-4}	7.7201×10^{-4}	9.3533×10^{-4}
		B	9.0339×10^{-4}	1.8873×10^{-4}	8.0917×10^{-4}
		C	7.6662×10^{-4}	3.6580×10^{-4}	9.1733×10^{-4}
	R	A	0.9996	0.9996	0.9995
		B	0.9995	0.9999	0.9996
		C	0.9996	0.9998	0.9995
	η		1	1	1

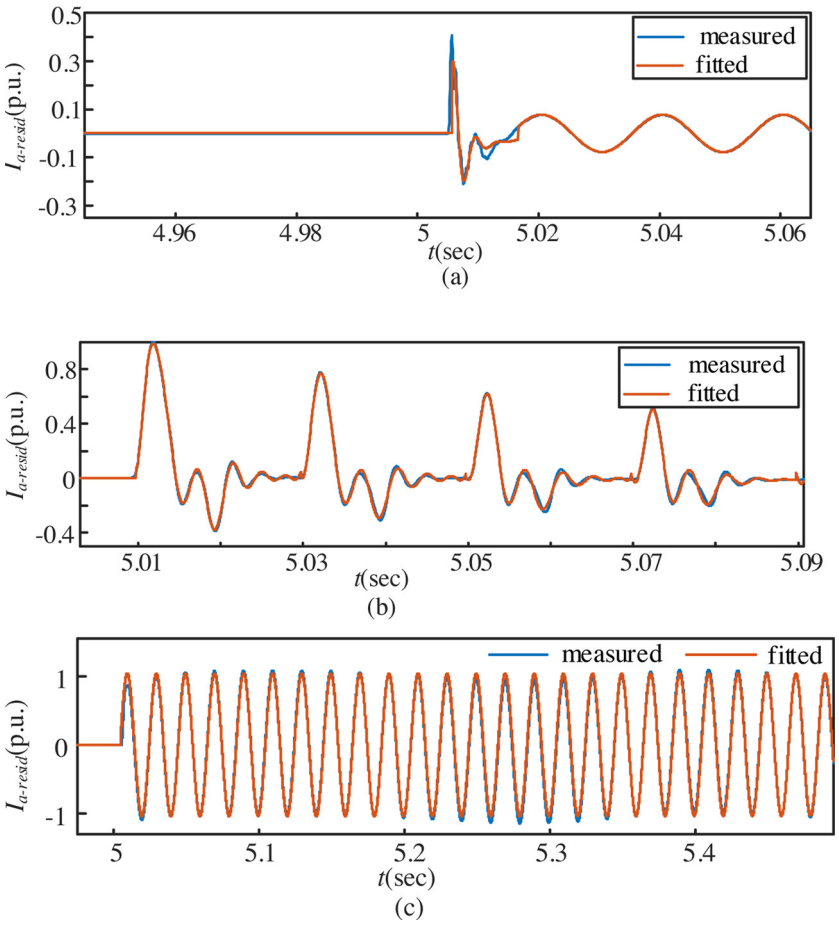

Fig. 8. The measured and fitted waveform (phase A) for the three disturbances. (a) Capacitor energization. (b) No-load transformer energization. (c) Motor starting.

Table 2
The fitness errors and the similarity degree of three phases.

	ε, η, R	A	B	C
Capacitor	ε	0.35%	0.09%	0.05%
	η	1	1	1
	R	99.82%	99.96%	99.97%
Transformer	ε	0.91%	0.45%	1.07%
	η	1	1	1
	R	99.55%	99.77%	99.46%
Motor	ε	0.08%	0.14%	0.16%
	η	1	1	1
	R	99.96%	99.93%	99.92%

represents the first phase template and $f_2(t)$ represents the second phase template, and sgn(t-s) is a sign function.

$$I_{resid-motor} = \frac{1-\mathrm{sgn}(t-s)}{2} f_1(t) + \frac{1+\mathrm{sgn}(t-s)}{2} f_2(t) \tag{13}$$

where

$$f_1(t) = A_{1m}(a-t)^{\alpha_{1m}} \cos[\omega_{1m}(t-a)+\theta_{1m}] + A_{2m}\cos(\omega_{2m}t+\theta_{2m}) \tag{14}$$

$$f_2(t) = A_{3m}e^{-\alpha_{3m}t}\cos(\omega_{3m}t+\theta_{3m}) + A_{4m}\cos(\omega_{4m}t+\theta_{4m}) \tag{15}$$

$$\mathrm{sgn}(t-s) = \begin{cases} -1 t \le s \\ 1 t > s \end{cases} \tag{16}$$

In Eq. (14), the first term represents a slow decaying oscillation mixed with the DC component, and the second term represents the steady-state sinusoidal component. In Eq. (15), the first term represents the fast decaying oscillation component at the fundamental frequency, and the second term represents the steady-state sinusoidal component. In Eqs. (14) and (15), A_{1m}, A_{2m}, A_{3m}, and A_{4m} are the magnitude, ω_{1m}, ω_{2m}, ω_{3m}, and ω_{4m} are the angular frequency, α_{1m} and a are the exponent and translation quantity of the power function. α_{3m} is the damping factor, θ_{1m}, θ_{2m}, θ_{3m}, and θ_{4m} are the initial phase angle.

In Eq. (16), s is the time that the motor starting enters the second phase and it is determined based on the difference between the maximum and minimum value in one power cycle, as shown in Eq. (17).

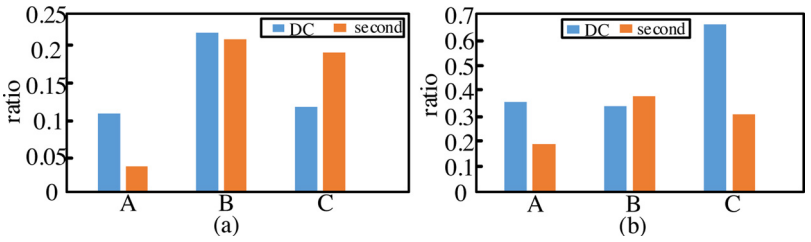

Fig. 9. The ratio between DC component, second order harmonic and the fundamental component. (a) Capacitor energization. (b) No-load transformer energization.

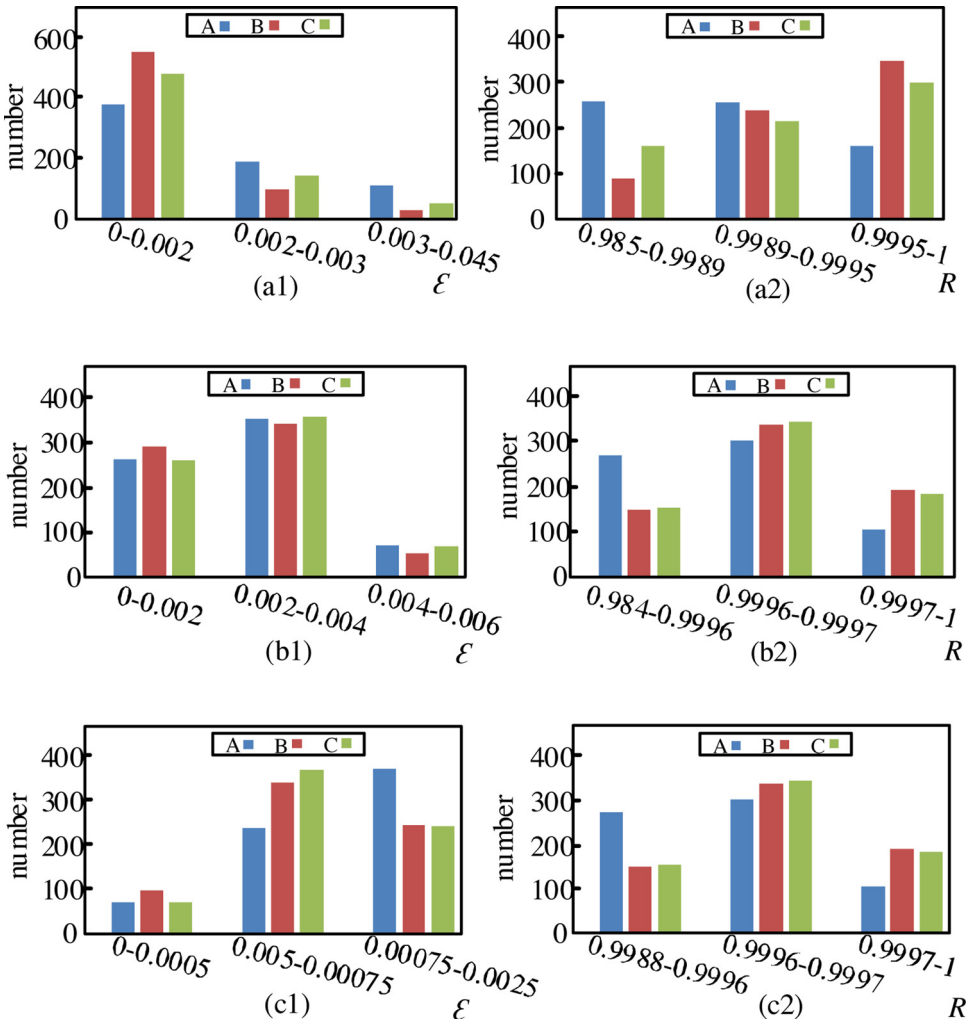

Fig. 10. The three-phase fitness error and similarity degree for all the 685 cases. (a1) and (a2) Capacitor energization. (b1) and (b2) No-load transformer energization. (c1) and (c2) Motor starting.

$$s = [(j-1) \times N_0] \times \Delta t \tag{17}$$

where N_0 is the number of sampling data point in one cycle and j is determined if the difference between the maximum and minimum value of the j-th cycle satisfy (18),

$$\frac{(x_1 - y_1) - (x_j - y_j)}{(x_1 - y_1)} \times 100\% > b \tag{18}$$

where, x_1 and y_1 are the maximum and minimum residual current value of the first cycle, x_j and y_j are the maximum and minimum value of the j-th cycle. Based on extensive simulations and field data tests, 25% is selected as the value of b in this paper. In practice, b can also be other values based on technicians' experience.

3.4. Flowchart of the proposed method

Based on the developed templates, the flowchart of identifying three energizing events is presented in Fig. 6. First, the abnormal waveform should be detected and extracted. Then, the residual current waveform is obtained by subtracting the first cycle from the saved waveform. Afterwards, each template is used to fit the obtained residual current waveform. If the fitness error is within a certain threshold and all parameters are significant, the root cause is identified.

1) Error calculation

In order to quantify the difference between the fitted residual waveform with the measured residual waveform, the normalized mean square error (NMSE) is used, which can be calculated by Eq. (19). The threshold of the error is set as 10% in this paper.

$$\varepsilon = \left[\sum_{i=1}^{L} (I_{resid\_}real(i) - I_{resid\_}fit(i))^2\right] / \left[\sum_{i=1}^{L} (I_{resid\_}real(i))^2\right] \tag{19}$$

In Eq. (19), I_{resid_real} and I_{resid_fit} are the measured value and fitted value of the residual current waveform and ε is the error.

2) Component significance

The small fitness error alone does not indicate a good match between the measured disturbance and the template. For example, if the 2nd to 5th harmonic components in the no-load transformer energization template are close to zero, this disturbance is unlikely to be caused by the no-load transformer energization even if the fitness error is very small. Thus, component significance should also be checked. The component significance is determined by the magnitude of each component in the template. If the magnitudes of one or more component are very small, it means the component is not significant, i.e. the recorded disturbance does not match well with the template even if the fitness error is small. In this paper, the estimated magnitude of each component is required to be greater than 0.01 p.u. The base value is determined by the rated capacity and rated voltage of the system. Here, η

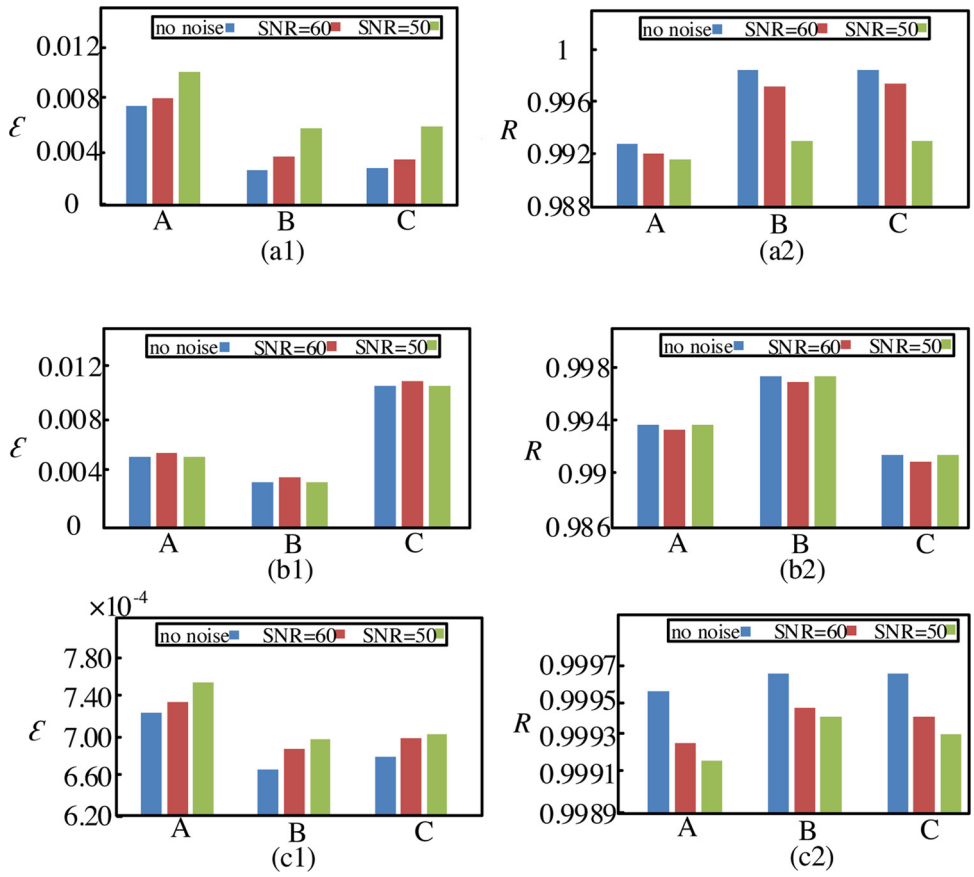

Fig. 11. The average fitness error and average similarity degree under different noise conditions. (a1) and (a2) Capacitor energization. (b1) and (b2) No-load transformer energization. (c1) and (c2) Motor starting.

Table 3
The test results of the proposed method for other disturbances.

		Capacitor energization			Transformer energization			Motor starting			Single-line-to-ground-fault		
Template	ε and η	A	B	C	A	B	C	A	B	C	A	B	C
Capacitor	ε (%)	0.35	0.09	0.05	**73.51**	**65.66**	**64.01**	**19.41**	**20.01**	**20.02**	**79.86**	**46.51**	**32.46**
	η	1	1	1	**0**	**0**	**0**	**0**	**0**	**0**	**0**	**0**	**0**
Transformer	ε (%)	0.11	0.02	0.01	0.91%	0.45%	1.07%	0.0016	0.0014	0.0020	0.02	0.36	0.09
	η	**0**	**0**	**0**	1	1	1	**0**	**0**	**0**	**0**	**0**	**0**
Motor	ε (%)	0.52	0.14	0.10	**58.98**	**52.22**	**71.92**	0.08	0.14	0.16	0.73	**52.85**	**61.36**
	η	**0**	**0**	**0**	**0**	**0**	**0**	1	1	1	**0**	**0**	**0**
Identification result		Capacitor energization			Transformer energization			Motor starting			Other disturbance		

The bold values mean that the error does not satisfy the threshold or the fitness does not pass the component significance test.

is used to represent the test result, i.e. if all the estimated magnitude is greater than 0.01 p.u., the fitness passes the component significance test and η equals one. Otherwise, η equals zero.

$$\eta = \begin{cases} 1, & \text{pass} \\ 0, & \text{fail} \end{cases} \tag{20}$$

3) Similarity degree calculation

In order to further characterize the similarity degree between the detected disturbance and the template, the correlation coefficient is calculated by Eq. (21). The index is similar as the correlation coefficient in the linear regression analysis.

$$R = \sqrt{1 - \frac{\sum_{i=1}^{L} (I_{resid\_}real(i) - I_{resid\_}fit(i))^2}{\sum_{i=1}^{L} (I_{resid\_}real(i) - \bar{I}_{resid-real})^2}} \tag{21}$$

In Eq. (21), $\bar{I}_{resid-real}$ is the average value of I_{resid_real}. R is the similarity degree. The higher the correlation coefficient is, the closer R is to one, and the more likely the root cause is identified accurately.

Mathematically speaking, the proposed approach is realized mainly by least square regression, which is performed by *lsqcurvefit* function in MATLAB. For a least square regression with N training samples, C parameters, and W iterations, its complexity is $O(WC^2N)$. Accordingly, the computational complexity for fitting three energization events can be analysed as follows.

3.4.1. Capacitor energization

Assuming the total number of data points in the saved time window is L, the number of unknown parameters in capacitor energization template is C_1, and the number of iterations is W_1, the cost of capacitor energization template fitting is $O(W_1C_1^2L)$.

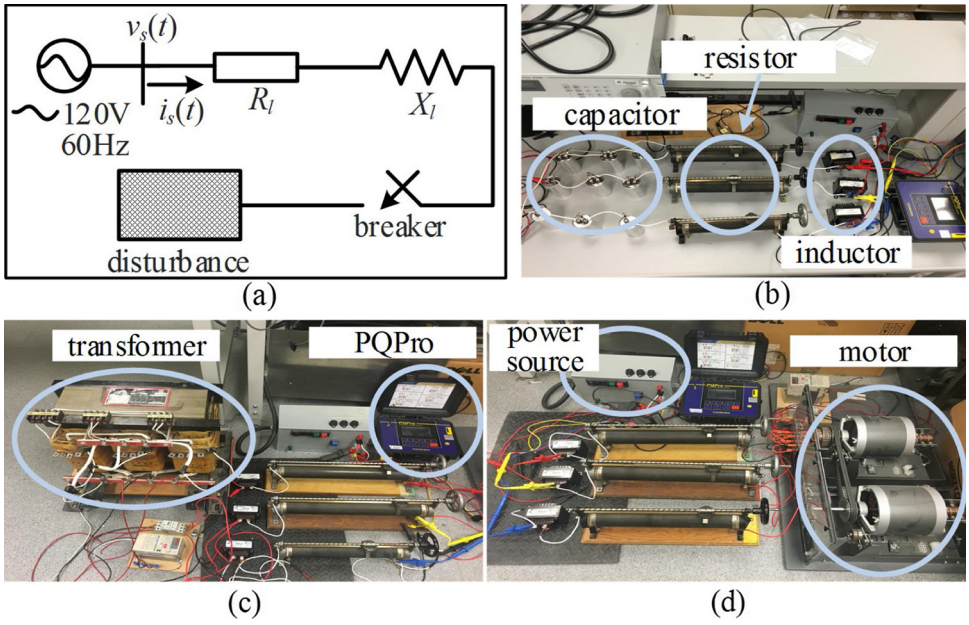

Fig. 12. The equivalent circuit and the photos of the lab experiments. (a) Equivalent circuit. (b) Capacitor energization. (c) No-load transformer energization. (d) Motor starting.

Table 4
The laboratory experiments test results.

Disturbance at original location		Capacitor energization			No-load transformer energization			Motor starting		
Template	ε and η	A	B	C	A	B	C	A	B	C
Capacitor	ε	0.76%	0.20%	0.26%	**91.41%**	**97.11%**	**85.99%**	**31.34%**	**31.86%**	**31.41%**
	η	1	1	1	**0**	**0**	**0**	**0**	**0**	**0**
Transformer	ε	0.09%	0.23%	0.47%	0.10%	0.095%	0.15%	0.016%	0.019%	0.006%
	η	**0**	**0**	**0**	1	1	1	**0**	**0**	**0**
Motor	ε	**29.08%**	**28.88%**	**31.25%**	4.55%	6.71%	9.24%	0.16%	0.24%	0.17%
	η	**0**	**0**	**0**	**0**	**0**	**0**	1	1	1
Identification result		Capacitor energization			No-load transformer energization			Motor starting		

The bold values mean that the error does not satisfy the threshold or the fitness does not pass the component significance test.

3.4.2. No-load transformer energization

Assuming L data points is divided into L/M segments (i.e. the number of data points in each segment is M), the number of parameters for the template fitting is C_2, and the number of iterations is W_2, the computational complexity of the no-load transformer energization template fitting is $O(W_2{*}L/M{*}C_2^2M) = O(W_2C_2^2L)$.

3.4.3. Motor starting

According to Eq. (13), the computational complexity of the motor starting template fitting with L data points is $O(W_3C_3^2L) + O(W_4C_4^2L)$, where W_3 and C_3 are the number of iterations and parameters in the first phase, and W_4 and C_4 are those in the second phase.

Besides of fitting three waveform templates, the error calculation for each template needs $O(L)$. Therefore, the total computational complexity of the proposed approach is $O(W_1C_1^2L) + O(W_2C_2^2L) + O(W_3C_3^2L) + O(W_4C_4^2L) + 3{*}O(L) = O(CL)$, where C is a constant and equals to $W_1C_1^2 + W_2C_2^2 + W_3C_3^2 + W_4C_4^2 + 3$. So far, the proposed method is used offline, thus its computational complexity is not a big concern. It is possible to develop its online application, but further research is needed.

3.5. Limitations of the proposed method

As seen from Fig. 6, the proposed method has clear physical meaning, thus its result can be trusted. However, it should be mentioned that there are two practical issues which may limit its application.

1) One premise to perform the proposed method is to detect the power disturbance with sufficient energy. This indicates the method may not work for the case where the energizing event is far away from the measurement point. This is in fact the challenge faced by all measurement-based methods.
2) The waveform template developed in the paper focuses on the single energizing event, thus is not applicable to the case where two energization events occurring simultaneously or immediately after another. However, we believe that the probability of the occurrence of the latter case is not very high.

4. Simulation studies

In order to verify the accuracy of the proposed method, simulation studies are conducted in the modified IEEE-13 node test system, as shown in Fig. 7.

The verification study considers four scenarios:

1) Several nodes are selected to energize different sizes of capacitors, no-load transformers and motors. The current recorded at the energizing location is used to fit the template developed in Section 3. The fitness error and the similarity degree are calculated.
2) Node 652 is selected as the energizing location, and the current recorded at the substation 650 is used to identify the root cause.

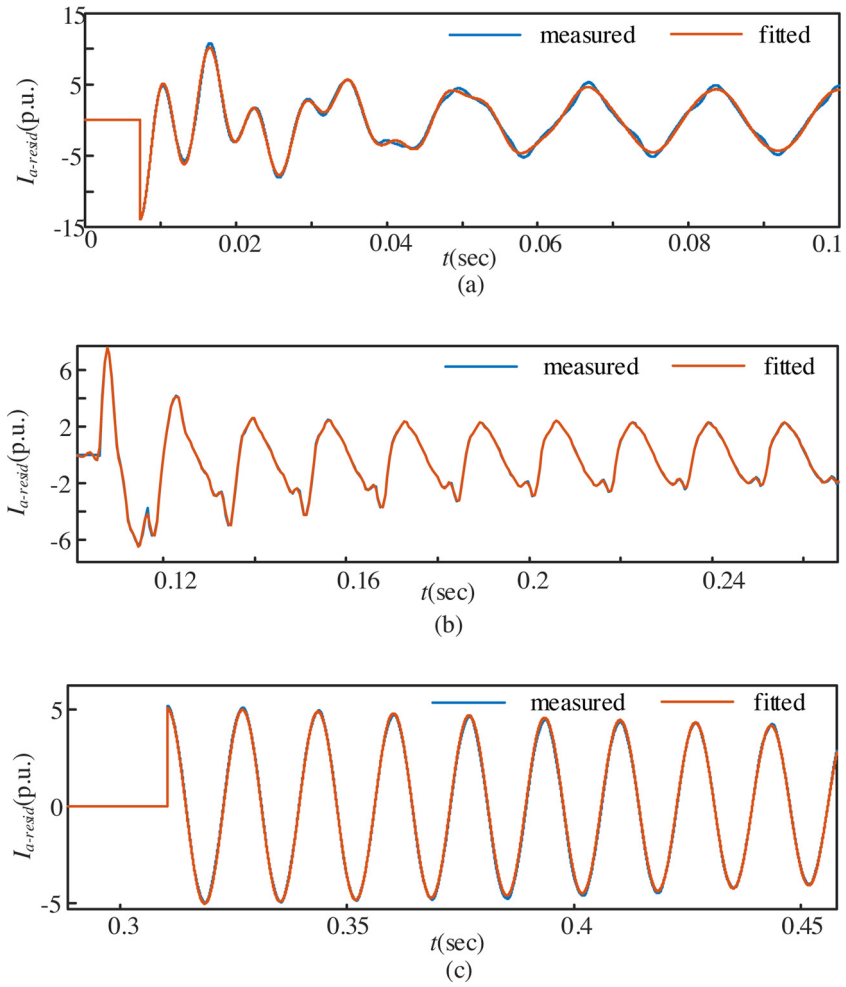

Fig. 13. The measured and fitted waveform based on the lab experiments.

3) Different switching locations, energizing capacities and switching instants are considered for energizing events. The effect of the measurement noise on the identification accuracy is also considered.
4) Other power disturbances such as single-phase-to-ground fault are simulated and fitted with the templates to test the robustness of the proposed method.

4.1. Identifying the root cause using disturbances recorded at energizing locations

In this subsection, node 680, 611, and 634 are selected as the energizing point. Capacitors, no-load transformers, and motors with different sizes are energized at different switching instants. The detailed information of simulation parameters is shown in Table 1. Based on the current measured at the energizing location, the residual current waveform can be obtained. The proposed method is then used to identify the root cause of the disturbance based on the flowchart shown in Fig. 6. The results are shown in Table 1.

As seen from Table 1, all root causes are identified correctly with small fitness errors and the similarity degrees close to one. The magnitudes of all components are greater than 0.01 p.u., i.e. the components pass the significance tests. Such results demonstrate that the proposed templates can characterize the features of the original disturbances properly.

4.2. Identifying the root cause using disturbances recorded at node 652

In this subsection, a 0.32 MVar capacitor, a 25 kV/0.4 kV 0.8136MVA no-load transformer, and an 814 kW motor are energized at node 652 respectively. The proposed method is then performed to identify the root cause based on the current measured at the substation 650. Fig. 8 shows the fitted residual current with the comparison of the measured one. The term “measured” indicates the residual current waveform obtained from the measurement, while “fitted” indicates the residual current waveform obtained by fitting the proposed template. Note this “measurement” can be done in field measurements, lab experiment or simulations.

As seen from Fig. 8, a good agreement can be observed. The fitness errors and the similarity degree are shown in Table 2. It can be seen that root causes are all identified correctly since fitness errors are small and the components pass the significance tests. This case study indicates that even if the disturbance is detected at the remote substation, the proposed method can still accurately identify the root cause.

Some existing methods identify the root cause of the disturbance based on the magnitudes of harmonic components. For example, [31] mentioned that the DC component and the second order harmonic for no-load transformer energization is generally between 15–20% of the fundamental component. However, as seen from Fig. 9(b), the second order harmonic of the no-load transformer energization could be higher than 20%. Besides, the capacitor energization could also induce power disturbances with similar harmonic components, as shown in Fig. 9(a). This finding indicates using empirical thresholds on harmonic components are not very robust in practice, as the magnitudes of harmonics change with the linear circuit.

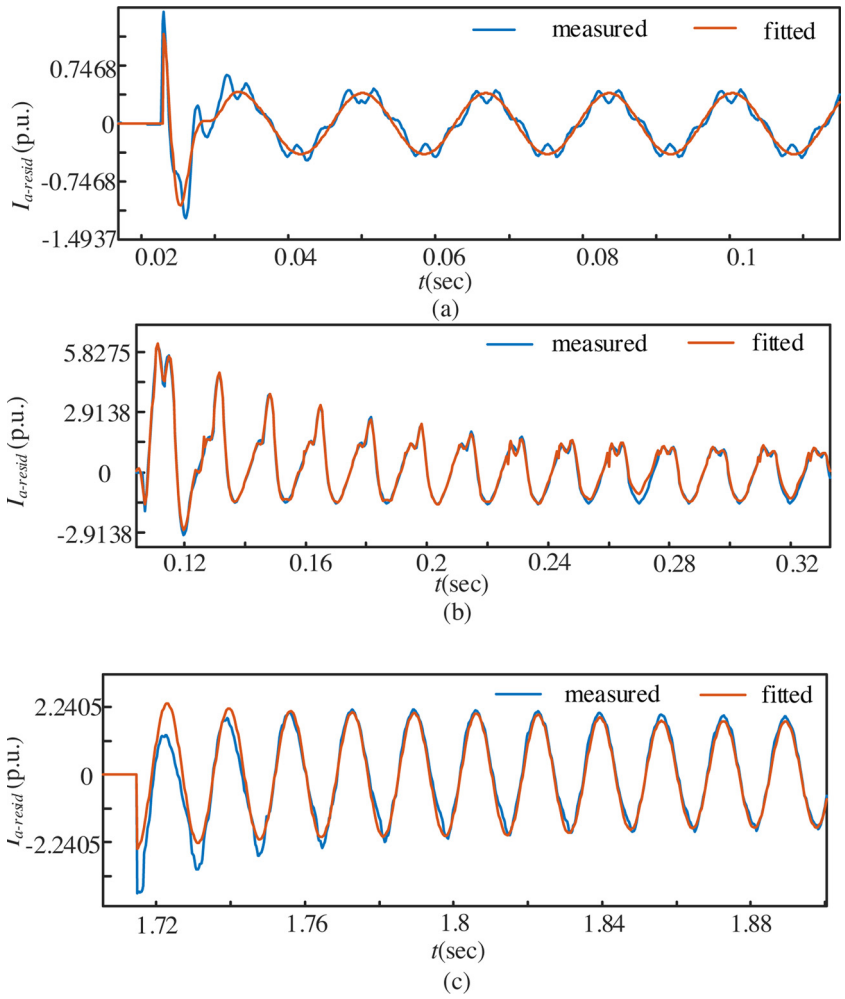

Fig. 14. The measured and fitted waveform (phase A) based on the field recorded data.

Table 5
The fitness errors, similarity degree and component significance test results of three phases.

Phase		A	B	C	Identification result
Capacitor	ε	7.88%	5.68%	5.93%	Capacitor
	η	1	1	1	
	R	0.96	0.97	0.97	
Transformer	ε	2.10%	1.095%	1.15%	Transformer
	η	1	1	1	
	R	0.99	0.99	0.99	
Motor	ε	2.34%	5.29%	2.01%	Motor
	η	1	1	1	
	R	0.99	0.97	0.99	

4.3. Identifying the root cause using disturbances recorded at various locations

The impact of switching locations, energization capacities, and switching instants are then studied. The switching locations cover all the 13 nodes. Based on the load size, the capacitor size ranges from 0.017MVar to 0.8MVar, the transformer size ranges from 0.034MVA to 1.77MVA, and the motor size ranges from 40 kW to 1.8 MW. The switching angle ranges from 0° to 360°. As a result, 685 cases are simulated for each disturbance. Fig. 10 depicts the errors and similarity degree for all the cases, in which the abscissa represents the fitness errors and similarity degree within certain range, and the ordinate represents the number of the corresponding cases. As seen from the abscissa in Fig. 10, all the errors are smaller than 5% and all the similarity degrees are greater than 98% for the three disturbances. The result indicates that the proposed method can accurately identify the root cause of three energizing events regardless of the switching locations, energization capacities, and the switching instants.

Additionally, the impact of the measurement noise on the proposed method is studied. The measurement errors with different signal-to-noise-ratio (SNR) are applied for the 685 cases of each disturbance. The average error and the average similarity degree under different noise conditions are shown in Fig. 11. As seen from the figure, the average errors are all smaller than 2%, and the average similarity degrees are all greater than 98.5%. Thus, it can be confirmed that the measurement noise has small impact on the proposed method.

4.4. Robustness of the template on other disturbances

In order to correctly identify the root cause of the disturbance, the developed template for each disturbance has to be unique. This subsection shows the result when fitting the developed template for other disturbances. Cross tests are conducted between capacitor energization, no-load transformer energization, and motor starting. Additionally, an extra disturbance, the single-line-to-ground fault is also studied. The results of the proposed methods are shown in Table 3. The bolded font means the value that does not satisfy the defined threshold, i.e. the reason why the disturbance cannot match the template. According to Table 3, the developed templates for three energization events are unique, i.e. only one root cause will be identified.

5. Laboratory test verification

In this section, laboratory experiments are further conducted to verify the proposed method.

5.1. Laboratory experiments set up

The equivalent circuit of the laboratory tests is shown in Fig. 12(a). The experiment equipment includes a 120 V three-phase voltage source, a waveform recorder (*PQPro*™ developed by CANDURA), capacitors (50 μF per capacitor), a transformer (30 kVA, 120/208 V), and a motor (175 W, 208 V, 1.3A). The photos of the laboratory experiment are shown in Fig. 12(b)–(d). The current $i_s(t)$ is recorded at the outlet of the power source.

5.2. Verification result

Based on the recorded current data $i_s(t)$, the proposed method is applied to identify the root cause of the disturbance. The results are summarized in Table 4. The comparison of the measured residual current waveform and the fitted waveform is shown in Fig. 13.

In Table 4, the bolded number means the identification result that does not satisfy the defined threshold. It can be seen all root causes of disturbances are identified correctly. Fig. 13 also shows that the fitted waveform matches the measured residual waveform very well.

6. Field data verification

This section demonstrates the performance of the proposed method using field data. For this purpose, the field data of three disturbances recorded at the substation are provided by the utilities, as shown in Fig. 14. The measurement was also taken by *PQPro*™ manufactured by CANDURA Instrument. The substation current is first stepped down by the ordinary current transformer at the substation and then measured by the current clamp of the *PQPro*™ instrument. The root cause identification result obtained by the proposed method is shown in Table 5. As seen from the table, all the fitness errors are within the threshold, and the similarity degree are greater than 95%. The results show that the proposed method can correctly identify the three disturbances in practice.

7. Conclusions

In this paper, a novel method to identify the root cause of three power disturbances, i.e. capacitor energization, no-load transformer energization, and motor starting, is proposed. The proposed method first develops the template for each disturbance based on their characteristics. Then, the developed templates are used to fit the disturbances recorded at the substation. The root cause of the disturbance is identified once the fitness is successful.

The proposed method has been verified by simulation studies and lab experiments. The impact of practical issues, such as switching locations, energization capacities, switching instants and the measurement noise has been studied. Finally, the performance of the proposed method is evaluated using the field data. The results indicate that the proposed method is robust and effective in practice.

The main contribution of this paper is to introduce a waveform-template based method for the root cause identification of power disturbances. The templates developed is not limited to three common energizing events. The future research will develop templates for other power quality disturbances.

Conflict of interest

The authors declare no conflict of interest.

Funding

1) the Research Initiation Fund of Zhejiang Sci-Tech University under grant (11132832611906). 2) the Fundamental Research Funds for the Central Universities under Grant (YJ201911).

References

[1] S. He, K. Li, M. Zhang, A real-time power quality disturbances classification using hybrid method based on s-transform and dynamics, IEEE Trans. Instrum. Meas. 62 (9) (2013) 2465–2473.
[2] K. Thirumala, T. Jain, A.C. Umarikar, Visualizing time-varying power quality indices using generalized empirical wavelet transform, Electr. Power Syst. Res. 143 (2017) 99–109.
[3] M. Uyar, S. Yildirim, M.T. Gencoglu, An effective wavelet-based feature extraction method for classification of power quality disturbance signals, Electr. Power Syst. Res. 78 (10) (2008) 1747–1755.
[4] J. Huang, Z. Jiang, L. Rylands, et al., SVM-based PQ disturbance recognition system, IET Gener. Transm. Distrib. 12 (2) (2017) 328–334.
[5] M.V. Reddy, R. Sodhi, A rule-based S-transform and AdaBoost based approach for power quality assessment, Electr. Power Syst. Res. 134 (2016) 66–79.
[6] F.P. Lima, A.D.P. Lotufo, C.R. Minussi, Wavelet-artificial immune system algorithm applied to voltage disturbance diagnosis in electrical distribution systems, IET Gener. Transm. Distrib. 9 (11) (2015) 1104–1111.
[7] D.D. Ferreira, J.M. de Seixas, A.S. Cerqueira, A method based on independent component analysis for single and multiple power quality disturbance classification, Electr. Power Syst. Res. 119 (2015) 425–431.
[8] T. Hubana, M. Saric, S. Avdakovic, Approach for identification and classification of HIFs in medium voltage distribution networks, IET Gener. Transm. Distrib. 12 (5) (2017) 1145–1152.
[9] C.N. Bhende, S. Mishra, B.K. Panigrahi, Detection and classification of power quality disturbances using S-transform and modular neural network, Electr. Power Syst. Res. 78 (1) (2008) 122–128.
[10] J. Li, Z. Teng, Q. Tang, et al., Detection and classification of power quality disturbances using double resolution S-transform and DAG-SVMs, IEEE Trans. Instrum. Meas. 65 (10) (2016) 2302–2312.
[11] S. De, S. Debnath, Real-time cross-correlation-based technique for detection and classification of power quality disturbances, IET Gener. Transm. Distrib. 12 (3) (2018) 688–695.
[12] H. Liu, F. Hussain, Y. Shen, et al., Complex power quality disturbances classification via curvelet transform and deep learning, Electr. Power Syst. Res. 163 (2018) 1–9.
[13] S. Santoso, W.M. Grady, E.J. Powers, et al., Characterization of distribution power quality events with Fourier and wavelet transforms, IEEE Trans. Power Deliv. 15 (1) (2000) 247–254.
[14] M. Karimi, H. Mokhtari, M.R. Iravani, Wavelet based on-line disturbance detection for power quality applications, IEEE Trans. Power Deliv. 15 (4) (2000) 1212–1220.
[15] H.Y. Zhu, S. Chen, Identification of capacitor switching transients with consideration of uncertain system and component parameters, IEEE Trans. Power Deliv. 23 (1) (2008) 213–220.
[16] O.P. Mahela, A.G. Shaik, N. Gupta, A critical review of detection and classification of power quality events, Renew. Sustain. Energy Rev. 41 (2015) 495–505.
[17] S. Khokhar, A.A.M. Zin, A.P. Memon, A new optimal feature selection algorithm for classification of power quality disturbances using discrete wavelet transform and probabilistic neural network, Measurement 95 (2017) 246–259.
[18] H. Eristi, O. Yildirim, B. Eristi, et al., Automatic recognition system of underlying causes of power quality disturbances based on S-transform and extreme learning machine, Int. J. Electr. Power Energy Syst. 61 (2014) 553–562.
[19] B. Li, Y. Jing, W. Xu, A genetic waveform abnormality detection method for utility equipment condition monitoring, IEEE Trans. Power Deliv. 32 (1) (2017) 162–171.
[20] IEC Electromagnetic Compatibility, Testing and Measurements Techniques – Power Quality Measurement Method, IEC 61000-4-30, (2015).
[21] A.G. Phadke, J.S. Thorp, Phasor Estimation at Off-nominal Frequency Inputs, Springer International Publishing, 2017, pp. 47–72.
[22] A. Ferrero, R. Ottoboni, A low-cost frequency multiplier for synchronous sampling of periodic signals, IEEE Trans. Instrum. Meas. 41 (2) (1992) 203–207.
[23] A. Cataliotti, V. Cosentino, S. Nuccio, A phase-locked loop for the synchronization of power quality instruments in the presence of stationary and transient disturbances, IEEE Trans. Instrum. Meas. 56 (6) (2007) 2232–2239.
[24] IEEE Working Group on Power Quality Data Analytics, Draft Report: Electric Signatures of Power Equipment Failures, Available: http://grouper.ieee.org/groups/td/pq/data/.
[25] M.M. Saied, Capacitor switching transients: analysis and proposed technique for identifying capacitor size and location, IEEE Trans. Power Deliv. 19 (2) (2004) 759–765.
[26] M. Merriman, A Text Book on the Method of Least Squares, 1st ed., Wiley Press, 1909.
[27] S.G. Abdulsalam, W. Xu, W.L.A. Neves, et al., Estimation of transformer saturation characteristics from inrush current waveforms, IEEE Trans. Power Deliv. 21 (1) (2006) 170–177.
[28] H. Gurocak, Industrial Motion Control: Motor Selection, Drives, Controller Tuning, Applications, 1st ed., John Wiley & Sons Press, 2015.
[29] H. Douglas, P. Pillay, A.K. Ziarani, A new algorithm for transient motor current signature analysis using wavelets, IEEE Trans. Ind. Appl. 40 (5) (2004) 1361–1368.
[30] V. Sit, M. Poulin-Costello, W. Bergerud, Catalogue of Curves for Curve Fitting, 1st ed., Forest Science Research Branch Press, Ministry of Forests, 1994.
[31] M. Jin, Y. Liu, A new inrush current identification algorithm based on transformer core saturation, Power Energy Soc. Gen. Meet. (2017) IEEE.